Iron–cobalt–graphite core–shell nanoparticles as efficient electromagnetic wave absorbers at X-band frequency range

Seyyed Salman Seyyed Afghahi[1], Ali Shokuhfar[2], Behzad Saberi[2], Abdollah Javidan[3]

[1]*Department of Engineering, Imam Hossein University, Tehran, Iran*
[2]*Department of Materials Science and Engineering, Advanced Materials and Nanotechnology Research Laboratory, K.N.Toosi University of Technology, Tehran, Iran*
[3]*Department of Basic Sciences, Imam Hossein University, Tehran, Iran*
E-mail: salmanafghahi@gmail.com

Published in Micro & Nano Letters; Received on 10th December 2013; Revised on 6th May 2014; Accepted on 13th May 2014

In this reported work, FeCo@C core–shell nanoparticles were synthesised using a novel two-step process. Characterisation of samples confirms the formation of graphite-coated FeCo nanoparticles. The electromagnetic wave absorption of nanocomposites containing 40%wt of FeCo@C and FeCo nanoparticles in the paraffin matrix was measured at 8–12.4 GHz frequency range. Two samples were prepared with thickness of 9 mm for FeCo and FeCo@C nanoparticles, respectively. Then the reflection loss was measured at ten different thicknesses between 9 and 1.4 mm by slicing the samples and measuring the scattering parameter S_{11} for each sample thickness using a metal backing. Results show that by graphite coating of FeCo nanoparticles the maximum reflection loss (−5.5 dB) grows up to four times higher (−19.2 dB) and the corresponding thickness reduces to half. The reason lies in active dielectric-magnetic loss mechanisms in FeCo@C nanoparticles.

1. Introduction: Core–shell magnetic nanoparticles are a class of hybrid materials with novel functionalities including optical, electromagnetic and biomedical applications [1–3]. An important functionality of carbon-encapsulated magnetic nanoparticles is their application as strong electromagnetic (EM) wave absorbers in the gigahertz frequency range. Owing to the rapid development of wireless technology it is necessary to develop advanced electromagnetic wave absorbers with light weight, strong absorption and a wide range of working frequency. Soft ferromagnetic nanoparticles, especially FeCo nanoparticles, are good candidates for this purpose because of their high saturation magnetisation, higher Snoek's limit and high permeability at frequencies in the gigahertz range [4–6]. Various efforts have been reported that use a non-magnetic highly dielectric shell (especially carbon) with soft ferromagnetic metallic nanoparticles to enhance their absorption capability because of suppression of eddy currents (i.e. increasing the relative complex permeability) in the core, interfacial polarisations and higher imaginary permittivity [7–10].

According to the transmission line model the reflection loss (RL) for a metal-backed absorber with a thickness (d) is simulated by the following equations [11]

$$\mathrm{RL} = -20\log\left|\frac{Z_{\mathrm{in}} - Z_0}{Z_{\mathrm{in}} + Z_0}\right| \tag{1}$$

$$Z_{\mathrm{in}} = \sqrt{\frac{\mu_r}{\varepsilon_r}}\tanh\left(\mathrm{j}\frac{2\pi f d}{c}\sqrt{\mu_r\varepsilon_r}\right) \tag{2}$$

Here ($\varepsilon = \varepsilon' - i\varepsilon''$) and ($\mu = \mu' - i\mu''$) are the complex permittivity and the complex permeability, respectively, Z_{in} is the input impedance when the electromagnetic wave incidence is normal to the absorber layer, f is the frequency of the incident wave, c is the velocity of light and Z_0 is the impedance of free space.

Equations (1) and (2) simulate the reflection loss at all thicknesses (d) using the permittivity and permeability, which are measured at a specific thickness of the absorber. Therefore, the effect of non-homogeneities of the nanocomposite absorber along its thickness, which is the intrinsic outcome of the sample preparation conditions, will not be taken into account. On this basis to measure the real operational absorptive properties of the prepared nanocomposites instead of using (2), the thickness of the sample should be changed at each stage (e.g. by wire cutting) and the reflection loss should be measured by the vector network analyser (VNA) at each thickness independently using the metal-backed approach. Then using (3), the reflection loss at each thickness would be obtained using the scattering parameter S_{11} which is directly measured by the VNA

$$\mathrm{RL} = -20\log|S_{11}| \tag{3}$$

The advantage of this processing method is in letting us measure the real absorptive properties of the nanocomposite absorber by taking the effect of microstructural inhomogeneities into account.

There are several methods to synthesise carbon-coated metallic nanoparticles including arc discharge [12], hydrothermal [13], thermal spray [14], magnetron and ion beam co-sputtering [15] and chemical vapour deposition methods [16]. Among these, chemical vapour deposition is a method capable of controlling the kinetics of carbon deposition by adjusting the reactive gas flow rate and the reaction time and temperature [17].

In the work reported in this Letter, we studied the effect of the carbon shell on the EM absorption of FeCo nanoparticles. We employed a novel two-step process including the microemulsion method and alcohol catalytic chemical vapour deposition (ACCVD) to synthesise FeCo cores and carbon shells, respectively. After inspecting the static magnetic properties of nanoparticles the performance of FeCo and FeCo@C nanoparticles were evaluated under the influence of electromagnetic waves in the range of 8–12.4 GHz. To determine the real operational performance of the prepared nanocomposite in which the effect of nanocomposite inhomogeneities are taken into account, the reflection loss of metal-backed samples was measured at each thickness independently.

2. Methods: Iron (III) chloride hexahydrate ($FeCl_3{\cdot}6H_2O$ (%99 +)), isooctane, 1-butanol, sodium borohydride ($NaBH_4$ (%99 +)) and cetyltrimethylammonium bromide (CTAB) were purchased from MERCK Chemicals and used as received with no

doi: 10.1049/mnl.2013.0723

further purification. Cobalt acetate tetrahydrate ($Co(CH_3COO)_2{\cdot}4H_2O$ (%99 +)) was supplied by MP Biomedicals. High purity nitrogen gas (%99.99 +) was used to provide an oxygen-free environment during the synthesis procedure. Ethanol as a carbon precursor was purchased from MERCK Chemicals and used with no further purification. High purity Ar + %10 H_2 gas (%99.99 +) was used to provide an oxygen-free environment during the ACCVD process, providing a suitable environment for growing graphite. FeCo nanocapsules were prepared using a two-stage process: (i) synthesis of FeCo nanoparticles using water in oil (reverse micelle) microemulsion and (ii) carbon coating of FeCo nanoparticles using the ACCVD method.

First, FeCo nanoparticles were synthesised using a quaternary microemulsion system at certain ratios of aqueous phase/surfactant/oil phase. Microemulsion 1 (ME1) and microemulsion 2 (ME2) were prepared on the basis of a quaternary phase diagram of water/CTAB, 1-butanol/isooctane which is described elsewhere [18]. $Fe_{70}Co_{30}$ alloy nanoparticles were prepared by mixing equal volumes of ME1 and ME2 containing metal salts and precipitating agent, respectively. A [water]/[surfactant] molar ratio of 37 was used. Moreover, the [$NaBH_4$]/[metal salts] molar ratio was kept at 2 to ensure that all precursors were reduced to zerovalent metal. ME1 was then transferred into a three-necked round bottom flask and then ME2 was added using a dropping funnel followed by vigorous stirring under N_2 atmosphere. Black precipitates of FeCo alloy nanoparticles appeared immediately after the mixing of two the microemulsions. After 10 min of reaction, the solution was centrifuged and washed with chloroform, ethanol and acetone several times to remove all residual elements.

FeCo nanocapsules were prepared via the ACCVD method. Dried FeCo powder was coated on a quartz boat and placed at the centre of a tube furnace (quartz tube, Ø ~ 5 cm). Then the reaction chamber was evacuated with a rotary pump to 10^{-4} Pa and purged with Ar + %10 H_2 for a few minutes and then gradually heated up to 750°C under the Ar + %10 H_2 atmosphere with a flow rate of 500 sccm. Subsequently, ethanol was introduced into the reactor by bubbling 500 sccmAr + %10 H_2 into the ethanol pool. The coating process was stopped after 30 min and the system was cooled down to room temperature under 500 sccm of Ar flow. Then some of the nanoparticles were exposed to acid etching by dispersing with vigorous stirring in Aqua Regia (HNO_3/HCl = 3/1) for 15 min to remove carbon soot and uncoated metal nanoparticles.

To investigate the power loss at the gigahertz frequency range FeCo@C core–shell nanoparticles were mixed with paraffin in a mould with dimensions of WR90 standard waveguide – which is used at a 8–12.4 GHz frequency range (X-band) – to make a paraffin matrix composite with 40%wt of nanoparticles. Then the reflection loss (RL) of the sample was measured at the 8–12.4 GHz frequency range using an Agilent 8510C VNA using a metal backing at thicknesses between 9 and 1.4 mm. At each stage the reduction in thickness was achieved using a copper hot wire.

Characterisation of samples was done using X-ray diffraction (XRD) (PANalyticalX'Pert Pro MPD with Cu k_α-radiation), a scanning transmission electron microscope (STEM) (ZEISS EM10-C at 100 kV) and a high-resolution transmission electron microscope (HRTEM) (JEOL JEM-2100 at 200 kV). Elemental analysis was done using an energy-dispersive spectroscopy (EDS) detector attached to the HRTEM. The magnetic properties of nanoparticles were evaluated using a room temperature vibrating sample magnetometer.

3. Results and discussion

3.1. Microstructural characterisation: Fig. 1*a* is the XRD pattern of as-synthesised FeCo nanoparticles. As observed, there is not any significant peak, which indicates the low crystallinity of as-synthesised nanoparticles because of the very fast borohydride reduction of metal salts. Fig. 1*b* confirms the formation of the

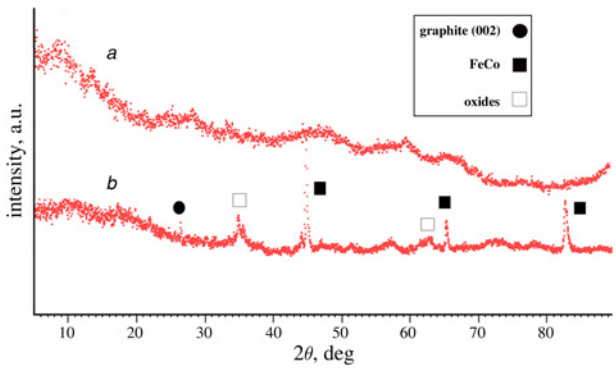

Figure 1 *XRD patterns for as-synthesised FeCo (pattern a) and carbon-encapsulated FeCo (pattern b) nanoparticles*

FeCo@graphite core–shell nanostructure. There are three main peaks (at $2\theta = 44.83°$, 65.32° and 84°) which are from (110), (200) and (211) lattice planes of α-bcc structured FeCo alloy. The only peak observed from graphite is the one at $2\theta = 26°$ relative to the (002) plane. Moreover, there are some oxide peaks which are because of the exposure of core particles to air.

Fig. 2*a* shows the TEM image of the FeCo core from the microemulsion method showing spherical nanoparticles with narrow size distribution. Fig. 2*b* shows the HRTEM micrograph for

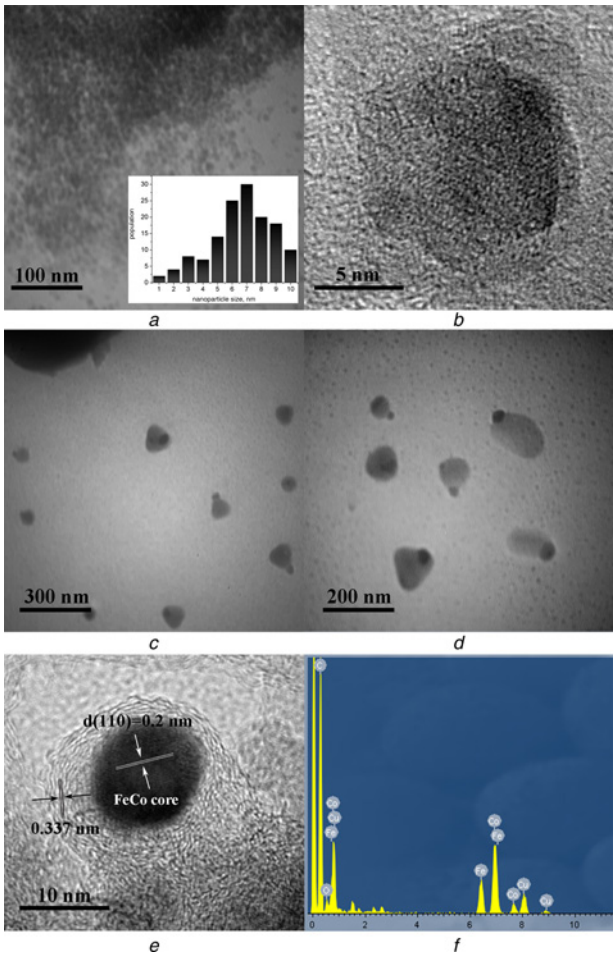

Figure 2 *TEM and HRTEM images of micelle synthesised FeCo nanoparticles (Figs. 2a and b); TEM images of FeCo@C nanoparticles prior to acid etching at two different magnifications (Figs. 2c and d); HRTEM of FeCo@C nanoparticle after acid etching (Fig. 2e); EDS spectrum of FeCo@C nanoparticles (Fig. 2f)*

as-synthesised FeCo nanoparticles. The low crystalline structure of FeCo nanoparticles is clearly visible which is in accordance with the XRD results. As seen from Figs. 2*c* and *d*, the cores are at the corner of each nanoparticle which means a directional growth of carbon. The onion-like structure of the coating is apparent from Fig. 2*e*. The interplanar spacing of 0.34 nm which is the characteristic of *c*-axis lattice distance between graphene sheets is shown in Fig. 2*e*. Moreover, the visible fringes in the core with a spacing of 0.2 nm are related to (110) planes of the α-bcc structured FeCo alloy. In fact, at the high temperature of the ACCVD process the amorphous FeCo as-synthesised nanoparticles have been subjected to coalescence and ripening to form larger crystalline FeCo cores. Fe, Co and C peaks in the energy-dispersive spectrum shown in Fig. 2*f* confirm the formation of graphite-encapsulated iron–cobalt nanoparticles.

3.2. Electromagnetic studies

3.2.1 M_s and H_c evaluation: Fig. 3 shows the hysteresis curves for FeCo and FeCo@C nanoparticles. FeCo nanoparticles exhibit superparamagnetic behaviour with zero coercivity but FeCo@C nanoparticles are ferromagnetic having finite coercivity. As seen from Fig. 3, FeCo@C nanoparticles show a higher saturation magnetisation than FeCo nanoparticles because of the growth of FeCo cores during the ACCVD process. It should be noted that the weak diamagnetic response of carbon shells could be neglected in the total magnetic properties of FeCo@C nanoparticles.

Moreover, the saturation magnetisation of both the samples are far less from the bulk value (~ 240 emu/g) mainly because of disordering of surface spins and incorporation of a magnetic dead layer as a small size effect [19, 20]. Since FeCo nanoparticles exhibit a superparamagnetic response they are in the single-domain size range. It should be noted that for single-domain magnetic nanoparticles the coercive field changes proportional to d^6 according to the following equation [21]

$$H_c = \frac{\alpha_1 K^4}{A J_s} d^6 \propto d^6 \tag{4}$$

However, in the multidomain size range the coercivity has an inverse relationship with the nanoparticle size [21]

$$H_c = \frac{\alpha_2 (AK)^{1/2}}{J_s d} \propto d^{-1} \tag{5}$$

where α_1, α_2 are the constant values, A represents the exchange stiffness, K the effective anisotropy constant, J_s the exchange energy density and d is the nanoparticle size.

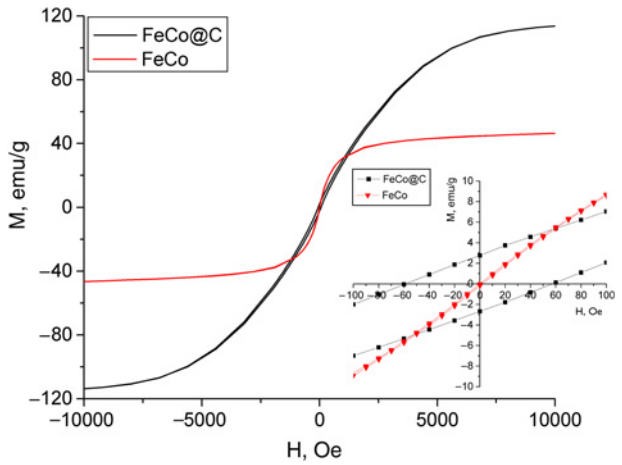

Figure 3 *Hysteresis curves for FeCo/FeCo@C nanoparticles*

Table 1 Magnetic properties of FeCo and FeCo@C nanoparticles with their corresponding sizes

Sample	Mean core size	Mean shell thickness	M_s	M_r	H_c
FeCo@C	30	12	113	3	60
FeCo	7	—	45	0	≅ 0

The dividing line between these two cases is the critical size D_{cr} in which the coercivity is maximum $D_{cr} = \pi S[J/Ka_0]^{1/2}$ where S is the spin moment per atom and a_0 is the lattice constant [22]. The critical size for FeCo nanoparticles is about 15 nm [23]. Therefore, the FeCo cores are in the multidomain size range. The magnetic properties of FeCo nanoparticles/nanoencapsulates along with their mean sizes are given in Table 1.

3.2.2 Electromagnetic wave absorption at X-band frequency range: One of the major functionalities of core–shell nanoparticles is their application as efficient electromagnetic wave absorbers especially in the microwave region. There are several magnetic and dielectric loss mechanisms which lead to dissipation of the EM wave. The magnetic loss is mainly because of ferromagnetic resonance, magnetic hysteresis, eddy current loss and domain-wall displacement, which promote the imaginary part (μ") of complex permeability ($\mu_r = \mu'_r - i\mu''_r$) [24, 25].

Dielectric loss mechanisms include electronic, ionic or orientation relaxations which result in increasing the imaginary part (ε") of complex permittivity ($\varepsilon_r = \varepsilon'_r - i\varepsilon''_r$) [5]. In the case of core–shell nanoparticles, it is possible to incorporate both dielectric and magnetic materials as core and shell or vice versa to achieve high values of dielectric and magnetic losses simultaneously. Moreover, some mechanisms like interfacial polarisation of space charges only activate when the material features a nanoscale-layered structure (e.g. core–shell structure) [26]. In this case, the redistribution of charges at the magnetic–dielectric interface dissipates a significant amount of energy.

Fig. 4 shows the RL for paraffin matrix nanocomposites containing 40%wt FeCo@C and FeCo nanoparticles at different thicknesses in the range of 8–12.4 GHz (X-band).

The maximum RL along with the effective absorption bandwidth (RL < −10 dB) at each sample thickness is given in Table 2. As

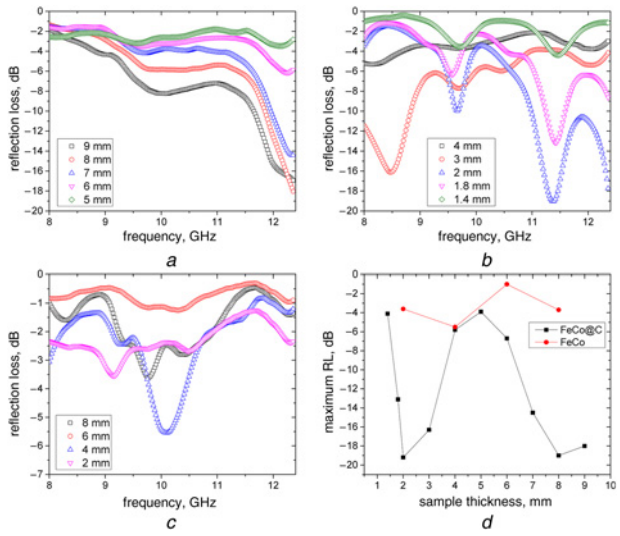

Figure 4 *Reflection loss at X-band for different thicknesses*
a and *b* FeCo@C/paraffin nanocomposites
c FeCo/paraffin nanocomposites
d Maximum RL for both samples at different thicknesses

doi: 10.1049/mnl.2013.0723

Table 2 Maximum RL and effective absorption bandwidth for FeCo and FeCo@C paraffin matrix nanocomposites at various thicknesses

Sample thickness, mm	RL max., dB		Bandwidth, GHz
	FeCo	FeCo@C	
1.4	—	−4.1	—
1.8	—	−13.1	0.4
2	−3.6	−19.2	1.4
3	—	−16.3	0.8
4	−5.5	−5.8	—
5	—	−3.9	—
6	−1	−6.7	—
7	—	−14.5	0.4
8	−3.7	−19	0.5
9	—	−18	0.8

shown by Figs. 4*a–c*, FeCo@C nanoparticles show very higher values of RL (up to −19 dB at 2 mm thickness) compared with FeCo nanoparticles whose maximum RL is −5.5 dB at 4 mm thickness. As mentioned above, the reason lies in the synergistic effects of the magnetic and dielectric loss mechanisms. For FeCo@C nanoparticles, the dielectric properties of graphite increases the total loss by dielectric relaxation of carbon atoms [5]. Moreover, as a result of the constructed core–shell interface the space charges alternatively redistribute between cores and shells with the alternation of the applied field.

In addition, the magnetic loss mechanisms in FeCo cores increase the total loss. The hysteresis loss is mainly caused by the time lag between the magnetisation vector and the external magnetic field, which is negligible in a weak applied field. Moreover, since the conductive FeCo cores are surrounded by carbon dielectric shells the eddy currents would be suppressed. Therefore, the main magnetic loss mechanism should be the ferromagnetic resonance.

According to the equation $f_r = (\gamma/2\pi)H_{\text{eff}}$ [27] in which f_r is the frequency of natural resonance, γ is the gyromagnetic ratio (2.8 MHz/Oe) and $H_{\text{eff}} = 4K/3\mu_0 M_s$, the anisotropy constant K for bulk α-FeCo alloy is about 10^{-6} J/m^3 [28]; therefore, the ferromagnetic resonance frequency should be in the megahertz range. However, for small nanoparticles (with size d) the effective anisotropy ($K = K_v + 6K_s/d$) which consists of volume (K_v) and surface (K_s) contributions, increases and the resonance frequency shifts to very higher frequencies compared with the bulk.

It is evident from Figs. 4*a* and *b* that by decreasing the thickness from 9 to 5 mm the RL decreases with an almost uniform shape. However, by decreasing the thickness below 4 mm two peaks appear in the RL curve. Moreover, it is observed that absorbing peaks shift to lower frequencies by increasing the sample thickness.

For FeCo nanoparticles, the dielectric losses are absent and only the magnetic mechanisms contribute to the total observed loss. Since all magnetic loss mechanisms like dipole relaxation or domain wall resonance are low-frequency phenomena they could not contribute to the observed loss of FeCo nanoparticles. The only high-frequency magnetic loss mechanism is the ferromagnetic resonance. As noted above for small nanoparticles the resonance frequency could be promoted to the GHz range. Therefore, the absorption peak observed in a 4 mm-thick sample is because of ferromagnetic resonance.

Besides, the secondary attenuation mechanism could be eddy current loss. In fact, for conductive nanoparticles which are isolated in a non-conductive matrix the eddy currents will be suppressed but in our case there is a finite probability for FeCo nanoparticles to aggregate during the paraffin mixing process leading to the formation of a conductive network.

From the electron theory, it is known that $\varepsilon'' = \sigma/2\pi\varepsilon_0 f$, where σ is the conductivity [29]. Formation of a conductive network increases the total electrical conductivity of the sample leading to a higher imaginary part of permittivity which means higher loss. However, the backward reflection which is produced by eddy currents reduces the RL, which justifies the low RLs observed in Fig. 4*c*. The best RL of −19 dB for FeCo@C nanoparticles is achieved for a 2 mm-thick sample, while for FeCo nanoparticles the maximum RL of −5.5 dB was achieved at 4 mm thickness. This means that FeCo@C nanoparticles feature a higher RL of about four times greater with compensative reduction of thickness to half.

It is seen from Fig. 4*d* that for both samples the maximum RL changes with thickness in an alternative manner. It could be proposed that at specific thicknesses the reflected wave from the metal backing is an odd multiple of the quarter wavelength ($\lambda/4$) and therefore it would be subjected to a partially destructive interference with the incident wave resulting in higher RL similar to that observed in resonant absorbers.

Finally, it could be concluded that carbon coating of FeCo nanoparticles using the two-step process including the microemulsion technique and the ACCVD process is an efficient way to synthesise novel functional nanomaterials as efficient electromagnetic wave absorbers in the microwave frequency region.

4. Conclusion: In this reported work, the synthesis of FeCo@C core–shell nanoparticles was done using a method combining the microemulsion technique with chemical vapour deposition. FeCo as-synthesised nanoparticles have an amorphous structure, which makes them unstable at the temperature of the CVD process, leading to coalescence and ripening to larger nanoparticles. A magnetic property assessment of nanoparticles shows that FeCo nanoparticles are superparamagnetic and therefore are single domain. However, larger FeCo cores exhibit ferromagnetic behaviour.

The real non-simulated reflection loss of FeCo@C and FeCo nanoparticles was evaluated at a frequency range of 8–12.4 GHz. Results show a much higher absorption for FeCo@C nanoparticles because of both dielectric and magnetic losses. The dielectric relaxation of carbon shells along with the interfacial polarisation of space charges contribute to the dielectric loss of the core–shell sample. Moreover, the ferromagnetic resonance of FeCo cores is the main magnetic loss mechanism. However, in FeCo nanoparticles, the eddy current loss is the main mechanism of electromagnetic wave dissipation. Finally, it could be concluded that FeCo@C nanoparticles are efficient functional nanoparticles which could be used to dissipate electromagnetic waves in the frequency range of 8–12.4 GHz.

5 References

[1] Vaidya S., Patra A., Kumar A., Ganguli A.K.: 'CdS@TiO_2 and ZnS@TiO_2 core–shell nanocomposites: synthesis and optical properties', *Physicochem. Eng. Aspects*, 2010, **363**, pp. 130–134

[2] Yu M., Hu J., Liu J., Li S.: 'Electromagnetic properties of multiferroicmagnetoelectric $BaTiO_3$–$Co_xFe_{3-x}O_4$ core–shell particles obtained by homogeneous coprecipitation', *J. Magn. Magn.Mater.*, 2013, **326**, pp. 31–34

[3] Covaliu C.I., Paraschiv G., Biriş S.Ş., *ET AL.*: 'Maghemite and poly-DL-alanine based core-shell multifunctional nanohybrids for environmental protection and biomedicine applications', *Appl. Surf. Sci.*, 2013, **285**, pp. 86–95

[4] Lu B., Dong X.L., Huang H., *ET AL.*: 'Microwave absorption properties of the core/shell-type iron and nickel nanoparticles', *J. Magn. Magn. Mater.*, 2008, **320**, pp. 1106–1111

[5] Liu X., Or S.W., Ho S.L., *ET AL.*: 'Full X–K_u band microwave absorption by FeMn/Mn_7C_3/C core/shell/shell structured nanocapsules', *J. Alloy Compd.*, 2011, **509**, pp. 9071–9075

[6] Wang B., Zhang J., Wang T., Qiao L., Li F.: 'Synthesis and enhanced microwave absorption properties of Ni@Ni_2O_3 core–shell particles', *J. Alloy Compd.*, 2013, **567**, pp. 21–25

[7] Liu X.G., Ou Z.Q., Geng D.Y., *ET AL.*: 'Influence of a graphite shell on the thermal and electromagnetic characteristics of FeNi nanoparticles', *Carbon*, 2010, **48**, pp. 891–897

[8] Liu Q., Cao B., Feng C., Zhang W., Zhu S., Zhang D.: 'High permittivity and microwave absorption of porous graphitic carbons encapsulating Fe nanoparticles', *Compos. Sci. Technol.*, 2012, **72**, pp. 1632–1636
[9] Liu X., Wing S., Sun Y., *ET AL.*: 'Influence of a graphite shell on the thermal; magnetic and electromagnetic characteristics of Fe nanoparticles', *J. Alloy Compd.*, 2013, **548**, pp. 239–244
[10] Xie Z., Geng D., Liu X., Ma S., Zhang Z.J.: 'Magnetic and microwave-absorption properties of graphite-coated Fe; Ni, nanocapsules', *Mater. Sci. Technol.*, 2011, **27**, pp. 607–614
[11] Naito Y., Suetake K.: 'Application of ferrite to electromagnetic wave absorber and its characteristics', *IEEE Trans. Microw. Theory Tech.*, 1971, **19**, pp. 65–72
[12] Jiao J., Seraphin S., Wang X., Withers J.C.: 'Preparation and properties of ferromagnetic carbon-coated Fe; Co; and Ni nanoparticles', *J. Appl. Phys.*, 1996, **80**, p. 103
[13] Wang Z., Xiao P., He N.: 'Synthesis and characteristics of carbon encapsulated magnetic nanoparticles produced by a hydrothermal reaction', *Carbon*, 2006, **44**, pp. 3277–3284
[14] Yu F., Wang J.N., Sheng Z.M., Su L.F.: 'Synthesis of carbon-encapsulated magnetic nanoparticles by spray pyrolysis of iron carbonyl and ethanol', *Carbon*, 2005, **43**, pp. 3018–3021
[15] Singh A., Lavigne P.: 'Deposition of diamond-like carbon films by low energy ion beam and dc magnetron sputtering', *Surf. Coat. Technol.*, 1991, **47**, pp. 188–200
[16] Kang J., Li J., Du X., Shi C., Zhao N., Nash P.: 'Synthesis of carbon nanotubes and carbon onions by CVD using a Ni/Y catalyst supported on copper', *Mater. Sci. Eng. A*, 2008, **475**, pp. 136–140
[17] Grüneis A., Rümmeli M.H., Kramberger C., *ET AL.*: 'High quality double wall carbon nanotubes with a defined diameter distribution by chemical vapor deposition from alcohol', *Carbon*, 2006, **44**, pp. 3177–3182
[18] Wang C.C., Chen D.H., Huang T.C.: 'Synthesis of palladium nanoparticles in water-in-oil microemulsions', *Physicochem. Eng. Aspects*, 2001, **189**, pp. 145–154
[19] Ma C., Luo B., Song H., Zhi L.: 'Preparation of carbon-encapsulated metal magnetic nanoparticles by an instant pyrolysis method', *New Carbon Mater.*, 2010, **25**, pp. 199–204
[20] Chen D.X., Pascu O., Roig A., Sanchez A.: 'Size analysis and magnetic structure of nickel nanoparticles', *J. Magn. Magn. Mater.*, 2010, **322**, pp. 3834–3840
[21] Luborsky F.E.: 'Development of elongated particle magnets', *J. Appl. Phys.*, 1961, **32**, pp. 83–171
[22] Ma M., Wu Y., Zhou J., Sun Y., Zhang Y., Gul N.: 'Size dependence of specific power absorption of Fe_3O_4 particles in AC magnetic field', *J. Magn. Magn. Mater.*, 2004, **268**, pp. 9–33
[23] Andra W., Nowak H.: 'Magnetism in medicine; a handbook' (Wiley-VCH, Germany, 2007, 2nd edn), pp. 550–567
[24] Murase K., Takata H., Takeuchi Y., Saito S.: 'Control of the temperature rise in magnetic hyperthermia with use of an external static magnetic field', *Phys. Medica*, 2013, in press, pp. 1–7
[25] Zhang T., Huang D., Yang Y., Kang F., Gu J.: 'Fe_3O_4/carbon composite nanofiber absorber with enhanced microwave absorption performance', *Mater. Sci. Eng. B*, 2013, **178**, pp. 1–9
[26] Li Y., Chen G., Li Q., Qiu G., Liu X.: 'Facile synthesis; magnetic and microwave absorption properties of Fe_3O_4/polypyrrole core/shell nanocomposite', *J. Alloy Compd.*, 2011, **509**, pp. 4104–4107
[27] Kittel C.: 'On the theory of ferromagnetic resonance absorption', *Phys. Rev.*, 1948, **73**, pp. 155–161
[28] Liu X., Morisako A.: 'Soft magnetic properties of FeCo films with high saturation magnetization', *J. Appl. Phys.*, 2008, **103**, pp. 07E726
[29] Ramo S., Whinnery J.R., Van Duzer T.: 'Fields and waves in communication electronics' (Wiley, India, 2007)

doi: 10.1049/mnl.2013.0723